The Binding Pocket at the Interface of Multimeric Telomere G-quadruplexes: Myth or Reality?

Francesco Manoli[+],[a] Filippo Doria[+],[b] Giorgio Colombo,[b] Barbara Zambelli,*[c] Mauro Freccero,*[b] and Ilse Manet*[a]

Abstract: Human telomeric DNA with hundreds of repeats of the 5′-TTAGGG-3′ motif plays a crucial role in several biological processes. It folds into G-quadruplex (G4) structures and features a pocket at the interface of two contiguous G4 blocks. Up to now no structural NMR and crystallographic data are available for ligands interacting with contiguous G4s. Naphthalene diimide monomers and dyads were investigated as ligands of a dimeric G4 of human telomeric DNA comparing the results with those of the model monomeric G4. Time-resolved fluorescence, circular dichroism, isothermal titration calorimetry and molecular modeling were used to elucidate binding features. Ligand fluorescence lifetime and induced circular dichroism unveiled occupancy of the binding site at the interface. Thermodynamic parameters confirmed the hypothesis as they remarkably change for the dyad complexes of the monomeric and dimeric telomeric G4. The bi-functional ligand structure of the dyads is a fundamental requisite for binding at the G4 interface as only the dyads engage in complexes with 1:1 stoichiometry, lodging in the pocket at the interface and establishing multiple interactions with the DNA skeleton. In the absence of NMR and crystallographic data, our study affords important proofs of binding at the interface pocket and clues on the role played by the ligand structure.

Introduction

Human telomeric DNA typically consists in a 4–15 kb long double-stranded (ds) region composed of 5′-TTAGGG-3′/3′-AATCCC-5′ repeats ending with a single-stranded (ss) 3′-overhang of some hundreds of nucleotides with the same repeating 5′-TTAGGG-3′ motif.[1] G-rich telomeric DNA can fold into G-quadruplex (G4) structures in solution and recent evidence has been obtained with a structure-specific G4 antibody, that the structure likely exists also in cells.[2] Human telomeric DNA plays an important role in various processes as it acts like a biological clock and shortens with aging.[2b,3] A protein complex, called Telomerase, is responsible for the maintenance of the telomere length in normal and cancer cells.[3] Being telomerase overexpressed in several types of cancer cells making them immortal, telomeric DNA has become an appealing target for the development of new therapeutic approaches.[4] To this end, a large number of molecules have been studied during the last decades for their potential to interact with human telomeric G4 structures.[5] Prior to biological assays affinity of new molecules for telomeric G4 s is assessed in solution mostly with the model telomeric DNA sequence, 5′-AGGG(TTAGGG)$_3$-3′, able to adopt a hybrid-1 G4 structure as main conformer in a K^+ rich solution (Scheme 1).[6] However, as telomeres consist in hundreds of nucleotides, we are witnessing an increase in the efforts to assess affinity of new ligands for multimeric telomere G4 structures of contiguous G4 blocks joined by the TTA linker as more reliable model.[7] One quest is the existence of a new type of binding site where two adjacent G4 units are connected.[8]

[a] *Dr. F. Manoli,[+] Dr. I. Manet*
Institute for Organic Synthesis and Photoreactivity (ISOF)
National Research Council (CNR)
Via P. Gobetti 101, 40129 Bologna (Italy)
E-mail: ilse.manet@isof.cnr.it

[b] *Dr. F. Doria,[+] Prof. G. Colombo, M. Freccero*
Department of Chemistry
University of Pavia
V. le Taramelli 10, 27100 Pavia (Italy)
E-mail: mauro.freccero@unipv.it

[c] *Dr. B. Zambelli*
Department of Pharmacy and Biotechnology
University of Bologna
V. le Fanin 40, 40127 Bologna (Italy)
E-mail: barbara.zambelli@unibo.it

[+] *These authors contributed equally to this work.*

Supporting information for this article is available on the WWW under https://doi.org/10.1002/chem.202101486

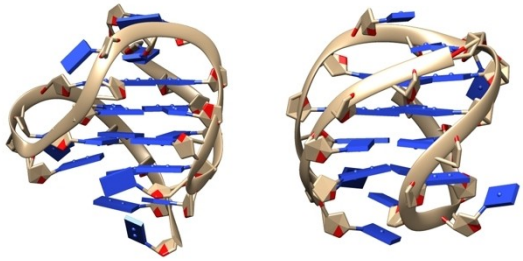

Scheme 1. Images of the hybrid-1 (left), and basket (right) G4 conformation of telomeric sequences (created with pdb entries 2GKU and 143D, respectively).

Crystal structures have not been reported neither for multimeric G4 telomeres nor for their complexes and also NMR data are lacking. In the absence of structural data several groups sought for alternative techniques to obtain information. The majority of the reported studies exclusively relying on ligand fluorescence intensity changes as function of the DNA concentration present strong limits as the intensity is strongly affected by the single binding site features.[7a,9] Other studies did not consider the importance of the binding stoichiometry, limiting the data analysis to the existence of the 1:1 complex, assuming the binding site to be at the interface of the adjacent G4 structures.[10] Very few studies corroborated the hypothesis of the existence and occupancy of the binding pocket at the G4 interface using a combination of techniques.[10a,11]

In this context we focused on various naphthalene diimide (**NDI**) ligands as G4 ligands. NDIs are extremely versatile compounds and their optoelectronic properties can be effectively tuned by substituents on the aromatic core.[12] This makes them appealing for biomedical applications exploiting their optical response.[13] We have published a series of monomeric NDIs with 3 or 4 ethyl or propyl side chains ending with an amine or quaternary ammonium function affording excellent water solubility and cellular entry, merged with promising features for theranostic applications.[13] In fact, nuclear uptake was evidenced by fluorescence confocal imaging exploiting the intrinsic NDI fluorescence and one displayed photocytoxicity upon irradiation with red light. Additionally, NDIs have been exploited as appealing scaffold for the design of G4 ligands, thanks to their chemical accessibility and large planar surface that can engage in stacking with the G nucleobases. For the above reasons NDIs have become well-known ligands for the telomeric hybrid-1 G4 structure (Scheme 1) as well as other G4 structures present in oncogene promoters. We and others have shown that tri-, tetra-substituted and core-extended NDIs are potent and reversible G4 ligands.[12d,14] Neidle et al. reported a series of NDIs, with alkyl side-chains linking a positively charged methyl-piperazine functionality to the NDI core, which significantly stabilize human telomeric G4 and inhibit the growth of several cancer cell lines at sub-μM concentrations.[14a,c,15] Some of them inhibited the telomerase complex in accord with the hypothesis that these NDIs act at the cellular level through telomeric G4 stabilization. Very recently, some of us investigated non-fluorescent NDIs selected from a small library by affinity chromatography (G4-CPG) assay as hTel46 G4 ligand with promising G4 vs. ds-DNA selectivity, but, they lack multimeric/monomeric-G4 selectivity.[16] We further explored this class of compounds producing a series of NDI dyads acting as fluorescent responsive ligands upon G4 binding.[17] Dyad ligands **1**–**2** (see Scheme 2) are very promising as they exhibited extremely low IC50 values for some cancer cell lines and induced DNA damage response, also at telomeric level, behaving very differently from the monomeric NDI analogues.[17] In an attempt to rationalize their ability to induce DNA damage at the telomeric level we decided to explore the binding of dyad ligands **1**–**2** to a dimeric telomeric G4 structure including NDIs **3** and **4** in the study as useful model to identify crucial ligand features in the binding process (Scheme 2). Our goal was to assess the role of the binding pocket at the interface as competitive binding site to the grooves or the G-tetrad ends. Using optical electronic spectroscopy and isothermal titration calorimetry (ITC) we determined the binding constants as well as the binding model for two telomeric sequences 5′-AGGG(TTAGGG)$_3$-3′ (hTel22) and 5′-GGG(TTAGGG)$_7$-3′(hTel45) in K^+ rich solutions. We performed a study of the fluorescence lifetime of the ligands in the presence of DNA as this parameter is very sensitive to the characteristics of the binding site micro-environment.[17a,18] Fluorescence lifetime data of the complexes, circular dichroism (CD) in the visible together with ITC thermodynamic parameters unequivocally proved that an additional binding site exists at the interface of contiguous telomeric G4s. In addition, modeling provided insights into the putative structural parameters that may play a role in this binding process. Noticeably, only the dyads engage in complexes with 1:1 stoichiometry, lodging in the pocket at the interface and establishing multiple interactions with the DNA skeleton.

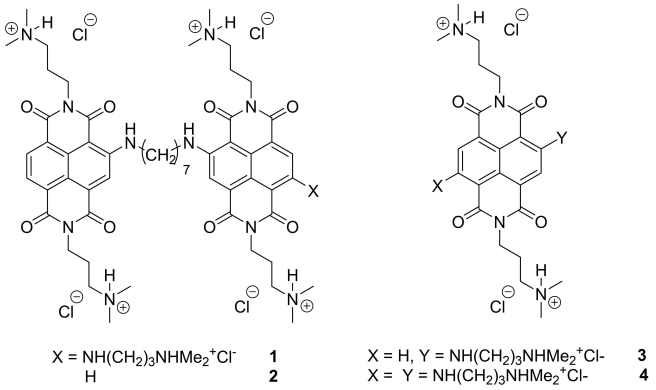

Scheme 2. NDI dyads **1**–**2** and monomeric NDIs **3**–**4** previously evaluated as G4 ligands.[17]

Experimental Section

The NDI molecules **1**–**4** shown in Scheme 2 were synthesized accordingly to published procedures.[17b] They were used for the binding study with two telomeric sequences 5′-AGGG(TTAGGG)$_3$-3′ (hTel22) and 5′-GGG(TTAGGG)$_7$-3′(hTel45) in K^+ rich solutions. DNA was acquired from Eurogentec. For titrations, keeping the NDI concentration constant, we monitored absorption, fluorescence, and circular dichroism spectra as well as the fluorescence decays with increasing amounts of DNA.

Absorption, CD and fluorescence spectroscopy

UV-visible absorption spectra were recorded on a Perkin Elmer λ650 spectrophotometer. Circular Dichroism (CD) spectra were recorded on a Jasco polarimeter J-715 accumulating 4 spectra with a scan rate of 50 nm/min (UV) or 100 nm/min (VIS). Fluorescence spectra were measured in right angle geometry using 1 nm steps and 0.5–1 s dwell time. Slits were set to 4–8 nm in excitation and 4–8 nm in emission. Where necessary a cut-off filter was used to eliminate Raman or excitation light. All the measurements were carried out at 295 K in quartz cuvettes with path length of 1 cm. All

fluorescence spectra were recorded for air-equilibrated solutions absorbing less than 0.1 to avoid inner filter effects and re-absorption of emission and corrected for wavelength dependent response of the monochromator/PMT couple. We excited at 495, 485, and 590, for **3**, **2**, and **4**, respectively, and 490 and 600 nm for **1**.

Fluorescence decays

Fluorescence decays were measured in air-equilibrated solutions for excitation at 465 nm (Horiba pulsed nanoled 1 MHz repetition rate) or 637 nm (Hamamatsu pulsed laser with 1 MHz repetition rate) using a time-correlated single photon counting system (IBH Consultants Ltd., Glasgow, UK) with a resolution of 55 ps per channel. Photons were detected in right angle geometry at 620 nm or 690 nm with a cut-off filter. Fluorescence decay profiles were analyzed with a least-squares method, using multiexponential decay functions (Eq. (1)) and deconvolution of the instrumental response function. Upon deconvolution form the instrumental response function the lifetime lower limit is 200 ps. The software package was provided by IBH Consultants Ltd.

The fitting function used is the following with j going from 1 to 3 or 4:

$$I(t) = b + \sum_{j=1}^{n} a_j e^{(-t/\tau_j)} \quad (1)$$

The relative amplitude α_j and the amplitude weighted average fluorescence lifetime, $<\tau>$ are calculated according to the following equations:

$$\alpha_j = a_j / \sum_{j=1}^{n} a_j \quad (2)$$

$$<\tau> = \sum_{j=1}^{n} \alpha_j \tau_j \quad (3)$$

If a fluorophore changes lifetime in different binding sites, the relative amplitude α_j equals the fractional concentration of the fluorophore in each binding site. For the fluorescence titrations a global analysis was performed of all decays including that of the NDI alone. The DAS software package provided by IBH Consultants Ltd was used to build a file with all decays. Next one decay was fitted with a 3- or 4-exponential decay function and the parameters of this fit were then optimized for all decays applying the same function. Eventually the converging global analysis afforded the optimized lifetimes together with the preexponential factors a_j for each decay. The lifetime of the free species is introduced as constant and is not further optimized.

Sample preparation for titration studies

For the spectroscopic measurements a 10 mM K^+ phosphate buffer of pH 7.0 was used, with 100 mM KCl. Stock DNA solutions of concentration of ca. 50 μM were prepared by dissolving the lyophilized compounds in a buffer solution containing 10 mM K-phosphate with 100 mM KCl of pH 7.0. The stock solutions were then heated at 90 °C for 15 min and slowly cooled to room temperature. The concentration of oligonucleotides was determined spectrophotometrically at 260 nm using molar absorption coefficient values ε of 228500 and 459500 $M^{-1}cm^{-1}$ for 5′-AGGG $(TTAGGG)_3$-3′ and 5′-GGG$(TTAGGG)_7$-3′, respectively. The molar extinction coefficients are calculated based on the nearest neighbor model. Based on melting curves monitoring absorbance at 260 nm the DNA concentration was corrected for absorption spectra measured at 25 °C. with 0.1 cm cuvettes. Aliquots of the dyad and DNA solutions dissolved in the same buffer were mixed together to prepare samples of varying molar ratio. Solutions were kept stirring in the dark for ca. 1 h before starting the measurements. Water was purified by passage through a MilliQ system (Millipore SpA, Milan, Italy). We excited at

Multiwavelength global analysis

The best complexation model, the binding constants as well as single spectra of the complexes were determined by means of a multivariate global analysis of multiwavelength data, analyzing a set of spectra corresponding to different dyad/DNA mixtures. We used the commercial program ReactLab™ Equilibria (Jplus Consulting Pty Ltd) developed in Matlab®. More details of the procedure are reported in the Supporting Information.

Isothermal titration calorimetry

NDI titrations were performed at 25 °C using a high-sensitivity VP-isothermal titration calorimetry (ITC) microcalorimeter (MicroCal LLC, Northampton, MA, USA). The reference cell was filled with deionized water. DNA and NDI solutions were prepared by diluting concentrated stock solutions in the reaction buffer (10 mM K^+ phosphate buffer of pH 7.0 with 100 mM KCl). In each individual titration, 10 μL of a solution containing **3**, **4**, **2** or **1** was injected into a solution of G4 DNA (hTel22 or hTel45), using a computer-controlled 310-μL microsyringe. All experiments were repeated two or three times to verify reproducibility and a control experiment was performed to evaluate the heat of dilution. Small endothermic effects for NDIs dilution into the buffer were observed more evident for **3** and **4** than for **1** and **2**, possibly indicative of disaggregation for **3**–**4** (Figure S6). The concentrations used in each experiment are reported in Table S3. To allow the system to reach equilibrium, a spacing of 210 s was applied between each ligand injection. For dyads titrations over hTel22 reloading the injection syringe was necessary to allow the binding to reach saturation.

Integrated heat data obtained for each titration were fitted using a nonlinear least-squares minimization algorithm to a theoretical titration curve, using Peaq software, using one or two sets of sites models. N (stoichiometry). ΔH (reaction enthalpy change, J mol^{-1}) and K_a (binding constant, M^{-1}) were the thermodynamic fitting parameters. The heat of dilution (J mol^{-1}) were also adjusted as fitting parameters. The reaction entropy was calculated using the relationships $\Delta G = -RT\ln K_a$ ($R = 8.3145$ J mol^{-1} K^{-1}, $T = 298$ K) and $\Delta G = \Delta H - T\Delta S$.

Computational approach

All docking runs were carried out using the Maestro software package (Schrödinger, LLC, NY, 2019). The ligands were manually drawn and then prepared for modeling by adding hydrogens and assigning bond orders. LigPrep (LigPrep, Schrödinger, LLC, New York, NY, 2019) and Epik (Epik, Schrödinger, LLC, New York, NY, 2019) were used to generate initial 3D geometries and all the possible stereoisomers. The most probable protonation and tautomeric states were calculated at pH = 7.0 ± 2. The target quadruplex structure was first analyzed using the SiteMap program of the MAESTRO suite. SiteMap identifies pockets that have structural and stereoelectronic features suitable to host a ligand molecule. Each ligand was docked by using the Glide module within the Schrödinger suite. A softened potential was used,

consisting in scaling the van der Waals radii. To preliminarily assess the viability of this approach for the present case, we previously proved that the protocol is able to reproduce the X-ray structure of G4-bound aromatic ligands as recent published:[16a] briefly, using structures in PDB 4DA3 and 2MB3, we deleted the experimentally solved ligands from the complexes. Next, we docked them back into the respective G4s. This procedure afforded as the best solution the correct binding poses observed in the PDB structures, with an RMSD between the predicted and experimental poses lower than 0.5 Å. While qualitative, the results of the docking approaches can thus be used as a means to interpret factors involved in recognition.

Results

To study the binding of these NDI ligands to the telomeric G4s, we performed titrations monitoring changes in absorption spectra, CD spectra, both in the UV assigned to DNA and in the visible due to NDI units, fluorescence spectra and decays. The experimental results were completed with a binding study using isothermal titration calorimetry (ITC). Table S1 shows some of the photophysical parameters of the ligands, previously reported,[17b] and relevant for the study reported hereafter.

Absorption titrations

Figure 1 shows the absorption spectra of all titrations and Figures S1a plot of the absorbance at single wavelengths vs. [DNA]/[ligand] ratio. Comparing the absorption spectra in Figure 1 of the monomers **3** and **4** with increasing amounts of hTel22 and hTel45 we observe in the visible range a hypochromic effect of ca. 40% for **3** vs. a small hyperchromic effect of 4% for **4**. Similarly, in the UV hypochromicity is more important for **3** than for **4**. Strong hypochromicity has been associated with intercalation of chromophores between base pairs,[18a] and, in case of G4 DNA, with π-π stacking of aromatic ligands with the planar G4 tetrads.[19] Therefore, **3** seems to prefer interaction by means of π-π stacking more than **4**, which is in line with the number of substituents and charge of the ligands both being larger in **4**. The latter with four positively charged substituents is more prone to electrostatic interactions with the backbone and suffers likely more from steric hindrance in π-π stacking.

We reported that the two NDI units of the dyad **1**–**2** strongly interact with each other as indicated by the low molar absorption coefficients compared to the monomers and the relative intensities of the peaks composing the visible absorption band (Table S1).[17b] The absorption spectra in Figure 1e–h of the dyads in the presence of hTel22 or hTel45 show important changes in the shape of the visible band and a significant increase of the absorbance of the lowest energy peak and are in line with disruption of the intramolecular interaction of the two chromophores. In the UV region, small changes can be observed differently from the strong hypochromicity observed for the monomers. The behavior is similar for both telomeric DNAs. The maxima of the visible absorption peaks close to 640 and 540 nm confirm interaction of both NDI units of the dyads with the DNA.[17b] Interestingly, in the absorption spectra of the dyad **1** the absorbance peak at 640 nm increases to a much greater extent compared to the 540 nm peak indicating that the tri-substituted and tetra-substituted unit interact differently with the two sequences. In the presence of dyad excess the baseline level increases due to aggregation of complexed species for both type of DNA.[17b]

Circular dichroism titrations

The CD spectra in the UV range have been recorded for all titrations. In order to appreciate the changes better they are shown in molar ellipticity in Figure S2 together with the molar ellipticity spectra of the two DNA that present the typical features of hybrid G4.[8] The changes in the CD spectra in the UV range (Figure S2) are similar in all cases. In the presence of ligand excess a small evolution toward antiparallel G4 structures can be envisaged as the ellipticity at 260 nm goes to zero or even below depending on the ligand. Both "basket" (Scheme 1) and "chair" antiparallel G4s have a UV CD imprint with a strong positive band at 295 and 245 nm and a negative at 265 nm, one G tetrad flanked by two lateral loops and one G tetrad with different ligand accessibility as it is covered by a diagonal loop in the basket and flanked by one lateral loop in the chair conformation.[20]

As the ligands used in this study are not chiral, we can only observe induced circular dichroism (ICD) signals due to asymmetry in the complex with G4. In the visible, we observe only for the dyads remarkably different features for hTel22 and hTel45 (Figure 2 and S3). In the case of hTel22 ellipticity is very low in all cases. Differently, an intense structured induced CD signal in the visible appears for the dyad **2** interacting with hTel45 (Figure 2b). Not only, there is also an inversion of the sign of the signal in the 320–400 nm region of the spectrum compared to hTel22. The same holds for **1** (Figure 2d) even though ellipticity is lower. The induced CD signal strongly depends on the local chirality experienced by the ligand and we can hypothesize a new binding environment for the dyads in the hTel45 complex.

Fluorescence titrations

Interesting features emerge also for the fluorescence properties of all NDIs upon complexation. The dyads have a low fluorescence quantum yield due to the interaction of the chromophores giving origin to nonradiative deactivation pathways of the excited state. Figure 3a–h shows the fluorescence spectra of the eight systems examined, in the presence of hTel22 or hTel45. In Figure S1 we plot the fluorescence intensity at single wavelengths vs. [DNA]/[ligand] ratio. In the case of **3** we observe total quenching for both hTel22 and hTel45, while in the case of **4** fluorescence is only partially quenched and, noticeably, recovers in the case of hTel45. The quenching of the fluorescence can be attributed to electron transfer in the

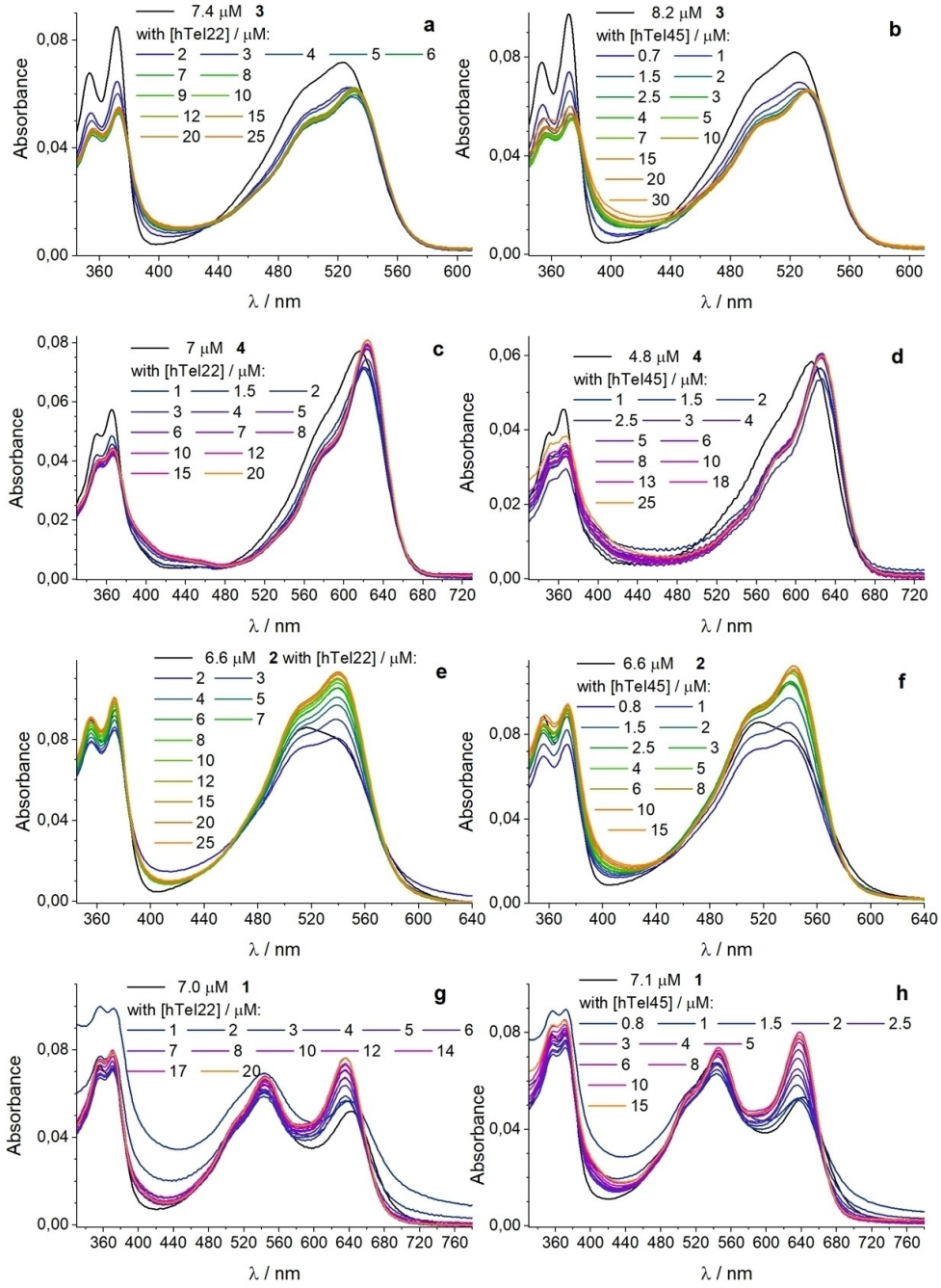

Figure 1. UV-Vis absorption spectra for titrations of **3** (a, b), **4** (c, d), **2** (e, f) and **1** (g and h) in the presence of increasing amounts of hTel22 (a, c, e, g) or hTel45 (b, d, f, h) in 0.01 M Phosphate buffer with 0.1 M KCl of pH 7; 1 cm cuvette.

complexes with **3** being less electron rich and thus a better electron acceptor compared to **4**.[17b,21] The best electron donor among the four bases is guanine, most easily oxidized, followed by adenine.[22] Photoexcited electron transfer depends further on proximity of the electron donor, in this case G or A, and acceptor, the NDI ligands, as well as their relative orientation.[21–23] Fluorescence of **2** is also strongly quenched and behaves differently with the two types of DNA, as in the presence of increasing amounts of hTel45, we observe a small intensity recovery together with a change in the shape of the spectra. The fluorescence of **1** is turned on as concerns the tetrasubstituted unit of the dyad (Figure 3g–h), while the trisubstituted unit is totally quenched (Figure S4i). These effects further confirm that interaction between the dyad chromophores is interrupted and the mode of G4 interaction of tri- and tetrasubstituted unit of the dyad differs.

We collected the fluorescence decays of all solutions with the different DNA amounts and performed a global analysis of all decays using a multi-exponential decay function. The fluorescence lifetime of a fluorophore is strongly environment

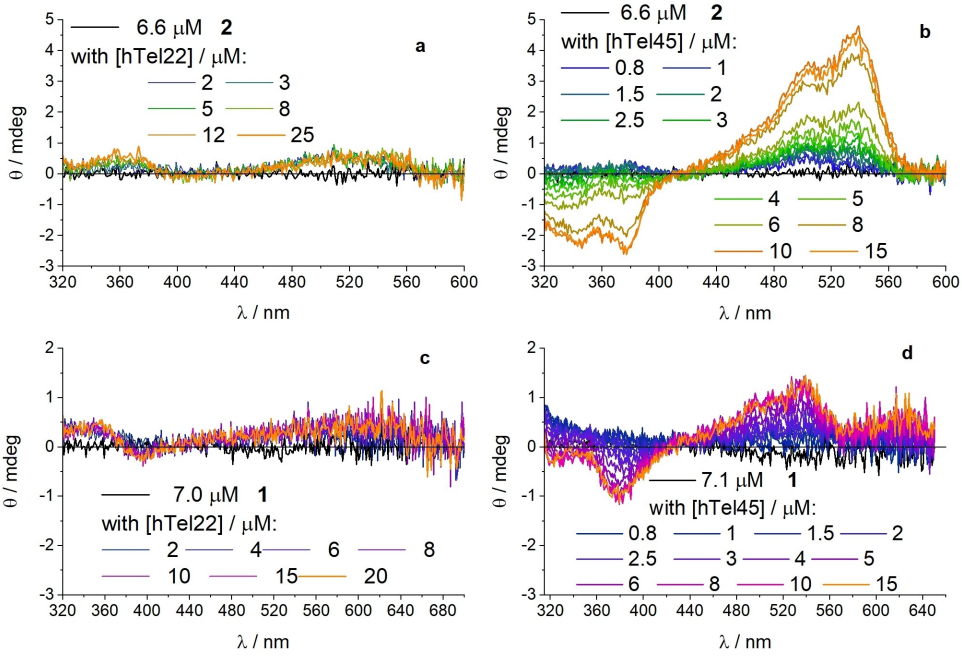

Figure 2. Visible CD spectra for titrations of **2** (a, b), and **1** (c, d), in the presence of increasing amounts of hTel22 (a, c) or hTel45 (b, d) in 0.01 M Phosphate buffer with 0.1 M KCl of pH 7; 2 cm cuvette.

dependent (so binding site dependent) and we expect lifetime values that change with the characteristics of the binding site. The analysis affords lifetime values and preexponential factors that allow to calculate the amplitude weighted average fluorescence lifetime, $<\tau>$, of each solution (Figure 4, red symbols). In case of multiple lifetimes of the same fluorophore experiencing different environments like different binding sites, the alfa values, α_j, in Equation (2) represent the fractional concentration of each emitting species. We needed a 3- or 4-exponential decay function to obtain convergence for the global analysis of all fluorescence decays of a titration.

In all cases a species with short lifetime close to the temporal resolution of the instrumental setup exists and is frequently the most abundant species. In the case of **4** and **1** we registered the appearance of a lifetime significantly longer than that of the free molecule. Interestingly, water molecules are able to shorten the lifetime of these fluorophores by vibronic relaxation (Table S1). So, lifetime lengthening may be indicative of reduced solvent exposure of the NDI in some binding sites on the DNA. Figure 4 depicts the results for global decay analysis of titrations shown in Figure 3 plotting the fractional concentrations (α_j) of the species with different lifetimes vs. DNA concentrations. The Y-axis on the right refers to the average fluorescence lifetime, $<\tau>$, varying along the titration.

We also fitted single decays at the end of titration with DNA present in excess, a condition relevant from the biological point of view, and the free species no longer present in solution (Table 1). Two or three lifetimes persist indicating the presence of species in two or three binding sites with different characteristics but similar affinity. Comparing the data for hTel22 and hTel45 for each ligand three interesting features emerge for hTel45 complexes: a very long lifetime of 8.0 ns and fractional concentration of 0.40 for **4**, a new lifetime of 0.7 ns and fractional concentration of 0.94 for **2**, and a new lifetime of 1.2 ns and fractional concentration of 0.61 for **1**. These data agree with the global analysis even though some alfa values slightly differ as global analysis comprises a more complex fitting including the free species lifetime. These new lifetimes suggest the presence of a binding site typical for hTel45, occupied to significant extent.

To rationalize all spectroscopic data, the software Reactlab™ Equilibria has been used to determine the binding model and the binding constants. Looking at single wavelength plots in Figure S1 and the lifetime data in Figure 4 the plots suggest in many cases the presence of more than one complexed species. More than one model has been tested and the best model has been identified comparing statistical outputs, aided also by the global lifetime analysis and the ITC data (See below).

Table 2 reports the binding constants as well as the models obtained from the fluorescence spectra analysis. Figure S4 shows the plots of the species concentration vs. total DNA concentration calculated with the optimized binding constants for all titrations. Comparison of the plots of the concentrations of the various species in solution vs. DNA concentration with the plots of the fractional concentrations of the lifetime global analysis vs. DNA concentration in Figure 4 was very useful as the trend in fractional concentration in many cases agreed with the trend in species concentration of both free and complexed NDIs in Figure S4. The binding constants do not exhibit a specific trend for neither type of DNA. As expected, a larger number of ligands can arrange in the dimeric G4 but we do not

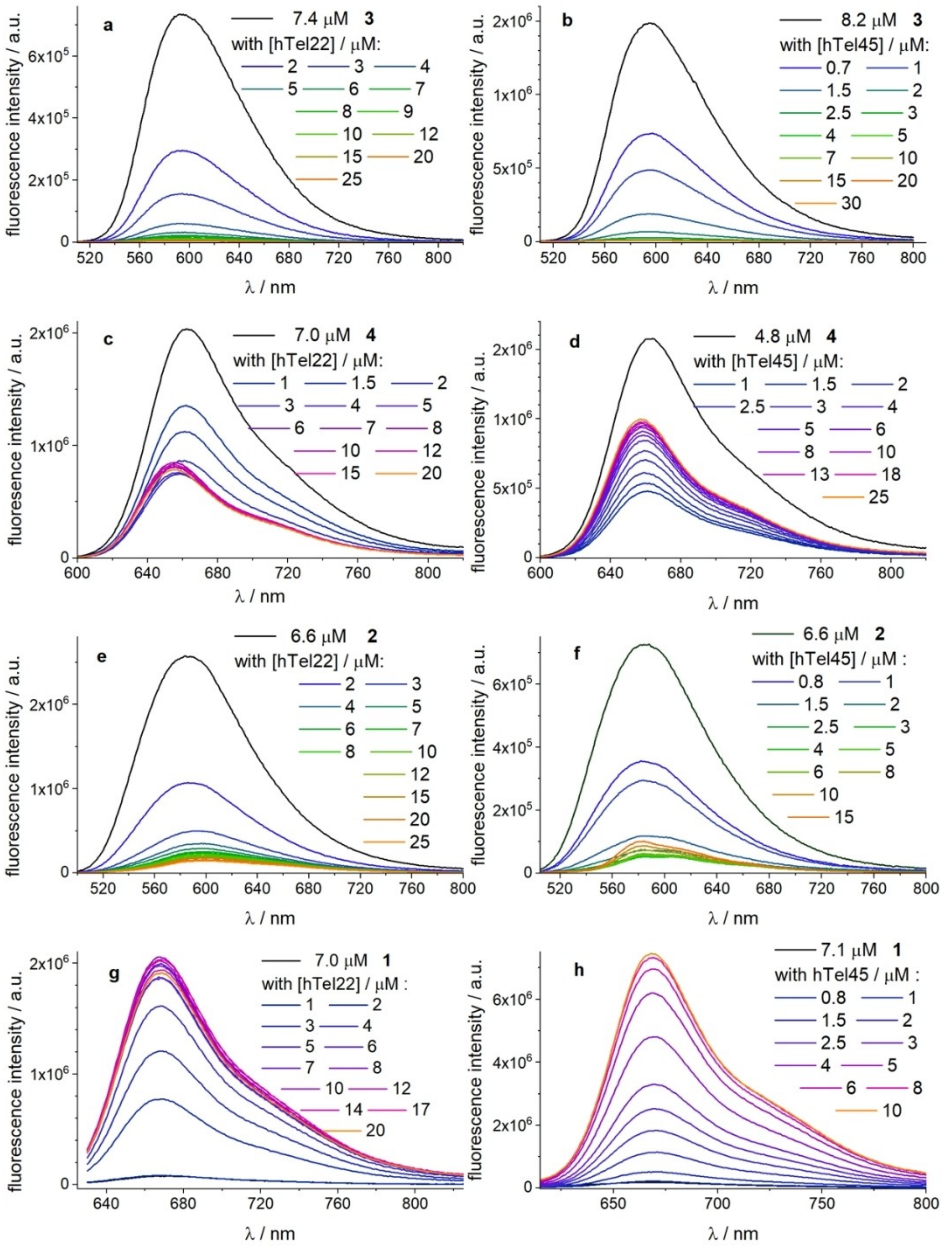

Figure 3. Fluorescence spectra for titrations of **3** (a, b), **4** (c, d), **2** (e, f) and **1** (g and h) in the presence of increasing amounts of hTel22 (a, c, e, g) or hTel45 (b, d, f, h) in 0.01 M Phosphate buffer with 0.1 M KCl of pH 7; 1 cm cuvette.

see any "doubling" effect in the number of ligands going from hTel22 to hTel45 neither a situation with "doubling plus one" due to the hypothetical new binding site at the interface between the two hybrid G4s. Likely the charge of the NDI ligands plays a relevant role in the number of molecules binding in high stoichiometry complexes. Indeed, we have 1:6 complex for **3** with charge 3^+ and 4:1 complex for **4** for charge 4^+. The analysis of the fluorescence spectra for **3** with increasing amount of hTel22 converges with a model of two complexes with 2:1 and 3:1 stoichiometry. In the case of binding to hTel45 we obtained convergence for absorption, fluorescence and visible CD with a single model of two complexes with 3:1 and 6:1 stoichiometry.

The fluorescence in the complexes is strongly quenched suggesting vicinity to G bases. If **3** binds in the G tetrad/lateral loop region, we envisage two such sites in hTel22 and three in hTel45 as electrostatic repulsion between the monomers may inhibit binding of two molecules in G tetrad regions at the G4 interface in hTel45. Further binding likely occurs in the groove regions in the complexes with higher stoichiometry. In the case of **4** analysis of the fluorescence spectra obtained for hTel22 and hTel45 yields a model with two complexes with 2:1 and 3:1 stoichiometry and with 2:1 and 4:1 stoichiometry, respectively. Both 2:1 complexes are fluorescent with relative yields comparable to that of the free molecule (Table S2 and Figure S5). The relative fluorescence yields represent an overall

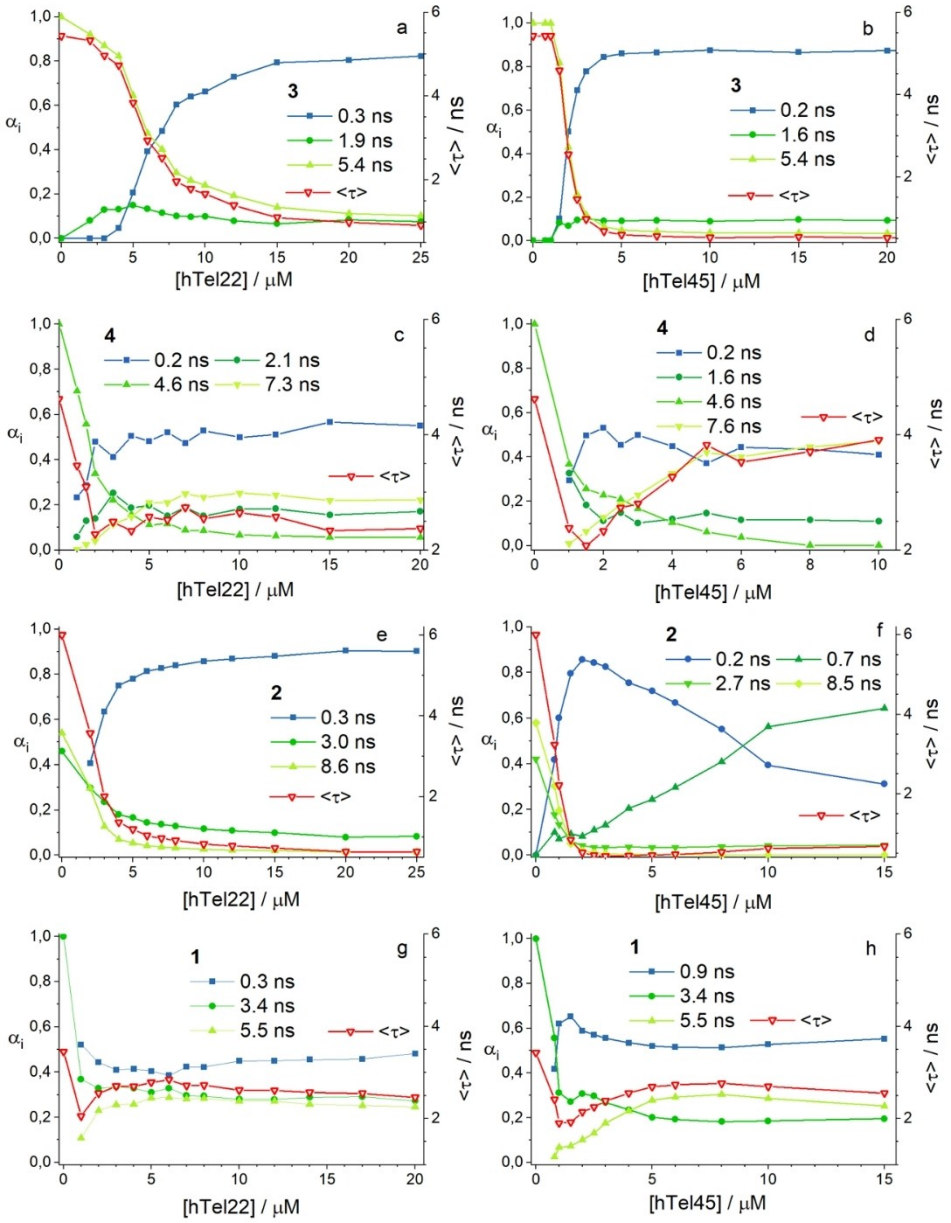

Figure 4. Plot of α_i values from global analysis, representing the species fractional concentration, vs. DNA concentrations. Right Y-axis refers to the average fluorescence lifetime $<\tau>$ (empty red triangles). Data were obtained from fluorescence decays of the solutions shown in Figures 1–3.

yield of the 2:1 complex and may hide individual differences in quantum yields for the two NDI molecules in the complex. They are in line with the existence of a species with a lifetime longer than that of the free molecule.

A very interesting frame emerges looking at the data of dyad **2**. For hTel22 only one complex with 2:1 stoichiometry exists, each binding site with a log*K* value of 6.45. Differently, for hTel45 a 1:1 complex exists with a slightly higher log*K* value, 6.62, and the log*K* value of the other dyads in the higher stoichiometry complex are 6.45. A similar situation emerges for dyad **1**, where in the presence of hTel45 also a complex with 1:1 stoichiometry exists with a log*K* value significantly higher than that in the 2:1 complex of hTel22. It is also higher than that of dyad **2** in the 1:1 complex of hTel45. Noticeably in the case of both dyads the complexation model emerging from the analysis of spectroscopic data is nicely confirmed by the lifetime data analysis. The average lifetime curves in Figure 4 stop changing at DNA concentrations where also the species concentrations remain constant (Figure S4). Moreover, the fractional concentrations of the species with 0.2 and 0.7 ns lifetimes observed for dyad **2** follow the trend of the 4:1 and 1:1 complexes, respectively. The fractional concentration of the species with 0.9 ns lifetime observed for dyad **1** follows the 4:1 complex concentration trend. The long 5.5 ns is typical of the complex and is likely present in both 1:1 and 2:1 complexes.

Table 1. Parameters of the fluorescence decay analysis of compounds **1**–**4** in the presence of the *highest* amount of hTel22 or hTel45 indicated in Figure 3.

	a_1, α_1	τ_1 (ns)	a_2, α_2	τ_2 (ns)	a_3, α_3	τ_3 (ns)
3	0.051	5.4				
3+hTel22	0.14, 81%	0.3	0.017, 10%	2.15	0.015, 9%	5.9
3+hTel45	0.19, 88%	0.2	0.02, 9%	1.7	0.006, 3%	5.8
4	0.16	4.6				
4+hTel22	0.16, 56%	0.2	0.055, 19%	2.4	0.069, 25%	7.2
4+hTel45	0.12, 48%	0.2	0.03, 12%	3.1	0.10, 40%	8.0
2	0.025	2.8	0.030	8.7		
2+hTel22	0.20, 90%	0.3	0.016, 7%	2.4	0.006, 3%	6.8
2+hTel45	0.11, 94%	0.7	0.007, 6%	2.7		
1	0.17	3.4				
1+hTel22	0.10, 42%	0.4	0.051, 21%	2.5	0.090, 37%	5.2
1+hTel45	0.045, 61%	1.2	0.029, 39%	5.15,		

Table 2. Binding constants obtained from the analysis of the fluorescence titration data and the ITC experiments.

Sample		Spectroscopy Complex Stoichiometry[a]	$\log K_{n:1}$	$\log K_i$ per site	ITC N	LogK
3	hTel22	2:1	13.31 ± 0.01	6.65	1.76 ± 0.02	6.64 ± 0.08
		3:1	18.05 ± 0.01	4.74		
	hTel45	3:1	21.98 ± 0.02	7.33	2.34 ± 0.05	7.5 ± 0.3
		6:1	40.38 ± 0.02	6.13	3.97 ± 0.05	5.63 ± 0.01
4	hTel22	2:1	14.04 ± 0.06	7.02	1.63 ± 0.02	6.96 ± 0.03
		3:1	19.76 ± 0.07	5.72	0.72 ± 0.01	5.97 ± 0.01
	hTel45	2:1	13.32 ± 0.01	6.66	2.23 ± 0.04	5.82 ± 0.01
		4:1	25.65 ± 0.02	6.16		
2	hTel22	2:1	12.88 ± 0.01	6.44	2.47 ± 0.04	6.6 ± 0.1
	hTel45	1:1	6.62 ± 0.05	6.62	0.85 ± 0.04	6.80 ± 0.05
		4:1	25.97 ± 0.03	6.45	0.75 ± 0.03	5.56 ± 0.003
1	hTel22	2:1	11.65 ± 0.02	5.82	1.53 ± 0.02	6.29 ± 0.01
	hTel45[b]	1:1	7.11 ± 0.04	7.11	0.32 ± 0.05	7.3 ± 0.3
		2:1	13.38 ± 0.04	6.27	1.07 ± 0.03	6.40 ± 0.01
		4:1	25.85 ± 0.06	6.23		

[a] ligand:DNA [b] the model was obtained from the analysis of the fluorescence spectra obtained for excitation at 490 nm, shown in Figure S3i

Isothermal titration calorimetry

The binding of ligands **1**–**4** to hTel22 and hTel45 has been investigated with ITC for the first time using the concentrations reported in Table S3. The NDIs were titrated into the DNA solution in the sample cell, exploring similar concentration ranges as the fluorescence studies, with some differences due to the titration scheme that, for the latter, encompassed DNA titration over NDIs. Heat of dilution titrating NDI molecules in buffer is shown in Figure S6. Table 2 reports the binding constants for each site, as well as the occupancy N, and Table 3 collects the thermodynamic parameters. Differently from fluorescence that keeps fixed the complex stoichiometry upon fitting, ITC analysis considers N values as variables, and may provide non-integer values. In all cases, the non-integer stoichiometry can be due to the known heterogeneity in G4 conformation of hTel22 and htel45, with the hybrid G4 conformation dominating in solution,[6,8b] and suggested by CD in the UV (Figure S2).

The ITC data for hTel22 show fair agreement with the fluorescence titration results both for monomers and dyads (Figure 5 A, B, C and D); for **3** and **4** both the stoichiometry and the affinity are maintained between the fluorescence and the ITC analyses (Figure 5A, B). In the case of **3**, the third binding event, with significantly lower affinity according to spectroscopy assays, is not detected by ITC (Figure 5A), likely because of the very low sigmoidicity of the binding isotherm at the concentrations used.[24]

The binding signatures show that while binding of the first two monomers is exothermic for both molecules, the third interaction observed for **4** occurs endothermically. Both events are entropically favored. From the spectroscopic titrations of the two dyads **1** and **2**, we know that aggregation of complexed G4s occurs at dyad excess above 3–4, therefore,

Table 3. Thermodynamic data from the ITC study, see Table S3 for concentrations.

	K_d (μM)	ΔH (kJ mol^{-1})	ΔS (J mol^{-1}K^{-1})	−TΔS (kJ mol^{-1})
hTel22 + **3**	0.23 ± 0.04	−15.1 ± 0.2	+76.4	−22.8
hTel45 + **3**	0.030 ± 0.003	−20.9 ± 0.2	+73.9	−22.0
	2.36 ± 0.01	−14.9 ± 0.3	+57.7	−17.2
hTel22 + **4**	0.11 ± 0.01	−10.2 ± 0.2	+99.0	−29.5
	1.07 ± 0.03	+5.4 ± 0.6	+132	−39.5
hTel45 + **4**	1.52 ± 0.01	−30 ± 2	+10.7	−3.2
hTel22 + **2**	0.26 ± 0.08	+6.5 ± 0.2	+148	−44.1
hTel45 + **2**	0.16 ± 0.02	−35.2 ± 0.6	+11.9	−3.6
	2.78 ± 0.02	−34 ± 4	−7.73	+2.3
hTel22 + **1**	0.52 ± 0.08	+13.2 ± 0.3	+165	−49.1
hTel45 + **1**	0.05 ± 0.04	−16 ± 10	+86.1	−25.7
	0.40 ± 0.03	−35 ± 4	+5.04	−1.5

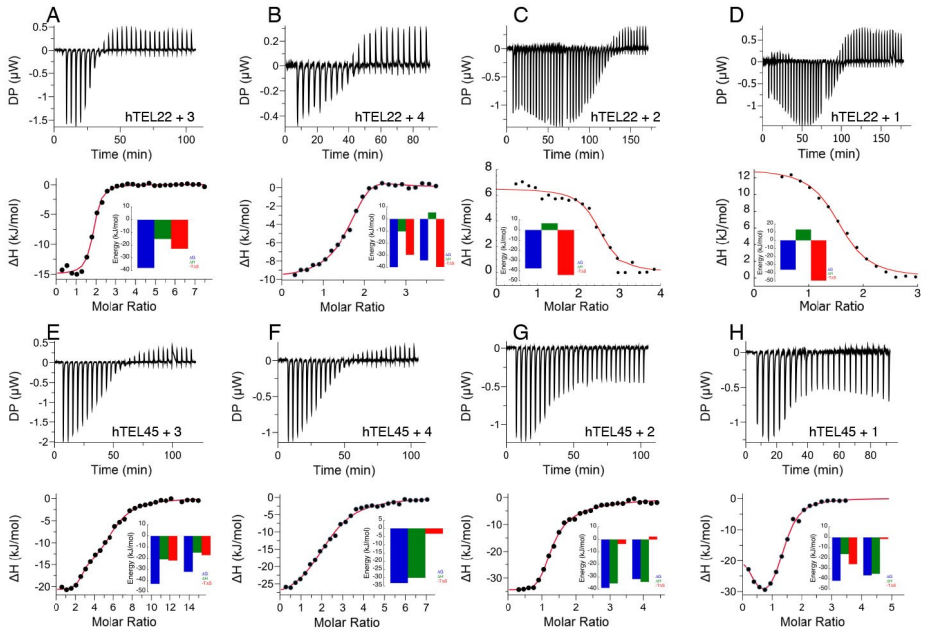

Figure 5. Representative experiments of titrations of **1**–**4** over G4 DNA molecules followed with ITC. In the upper panels the raw data are reported, while in the lower panels the integrated heat data (filled circles) and the best fit obtained (solid red line) are shown as a function of ligand/DNA molar ratio. Inserts represent the binding signature for each binding event (blue bar: ΔG; green bar: ΔH; red bar: $-T\Delta S$).

both curves were fitted up to a ratio 4:1 of dyad:DNA concentration (Figure 5C, D and Figure S7), showing substantial agreement with the spectroscopic results. Two dyads bind one DNA molecule with similar affinities for **1** and for **2**. Notably, ITC data indicate an endothermic binding for both titrations, while the entropic term is maintained positive.

The ITC binding study on hTel45 afforded some important data suggesting binding in the pocket at the G4 interface. Data in Figure 5E of **3** titrated with hTel45 show two types of different sites occupied by two and four molecules, respectively, with a maximal stoichiometry of six NDIs per DNA, consistent with the fluorescence titration analysis. Binding of **3** is enthalpically and entropically driven, with similar thermodynamic parameters for the two DNAs. For **4**, ITC only detects a single binding event with two-three molecules bound per hTel45 unit (Figure 5F), with affinity slightly lower than observed for fluorescence spectroscopy and negative enthalpy and entropy terms. A second binding event, observed in the spectroscopic analysis, is not visible in ITC, possibly associated to an adiabatic reaction. For the homologous dyad **2** (Figure 5G), a first binding event of one molecule per DNA occurs with similar thermodynamic parameters as the corresponding monomer and is consistently detected both by fluorescence and ITC experiments. A subsequent binding event of one NDI per DNA, occurring with lower affinity and unfavorable entropic term, is not consistent with spectroscopic data, which found a 4:1 complex. This may be due to the different concentration ranges of the two experimental approaches, with fluorescence assays reaching an excess of eight molecules per DNA, instead of four reached by ITC. For the binding of the dyad **1** to hTel45, ITC detects two binding events with affinities very similar to what observed in the spectroscopic analysis. The half integer stoichiometry observed for the first binding event under large DNA excess might be due to dimer formation with one dyad

bridging two DNA molecules.[25] This effect is not visible in fluorescence spectroscopy possibly due a much lower excess of DNA.

Comparison of the thermodynamic parameters for hTel22 and hTel45 (Table 3) gives a strong hint on a new binding site in hTel45. Indeed, binding of **2** and **1** to hTel45 gives enthalpy and entropy values for the site of highest affinity that strongly differ from the thermodynamic parameters in hTel22 binding. A favorable enthalpic contribution becomes dominating for **2** and **1** binding to hTel45, while the entropy contribution loses in weight. An energy penalty is possible as the interaction between the two NDIs needs to be interrupted for complexation, a feature emerging from the absorption spectra, and may be the origin of unfavorable enthalpy for hTel22 binding. In the case of monomeric ligands **3** and **4** the observed difference is not relevant or less distinct, respectively, confirming that these molecules bind in similar sites in hTel22 and hTel45 complexes of low stoichiometry.

Computational analysis

To rationalize the observed binding of the NDIs **1**–**4** to multimeric telomeric G4, we set out to obtain structural information of the complexes using a computational approach. The htel46 dimeric G4 structure obtained through molecular dynamics simulations by Hu et al.[7a] was used as the target in this study. First, we identified possible binding pockets on the dimeric G4 target sequence with stereoelectronic properties suitable to accommodate potential ligands, using the SiteMap program of the MAESTRO suite. Next, docking calculations were performed in the identified binding pockets, using the Glide program of the MAESTRO suite. SiteMap identified two potential binding sites (see Figure S8). The first, and more extended one, was located at the junction between the two G4 monomers, displaying a well-defined potential pocket at the interface between the two G4 motifs (Figure S8A). This pocket also extends into the groove presented by one of the two monomeric G4s. The second potential binding site appeared to be located on the surface of one monomer. Interestingly, the docking runs returned favourable binding poses only for the pocket at the interface (Figure 6), while no binding pose with favourable docking energy was retrieved for the second binding site.[26] The binding poses for **1** and **2** are shown in Figure 6B and 6 A, respectively. Those for NDIs **3** and **4** are depicted in the Supp. Inf. (Figures S9 and S10). Analysis of the binding poses indicate that the four compounds fit into the pocket. In agreement with the spectroscopic data, the computational analysis suggests that the binding unit is always the tri-substituted moiety, for both dyads **1** and **2**, which occupies the pocket at the junction between the two G4 domains (See Figures S11 and S12). The same pocket is occupied by the aromatic moiety of monomeric **3** and **4**, albeit with a slightly different pose (Figures S7 and S10).The monomeric NDIs **3** and **4** productively occupy the pocket with the aromatic substructure of the molecule involved in hydrophobic and partial stacking interactions, two of the ammonium substituents

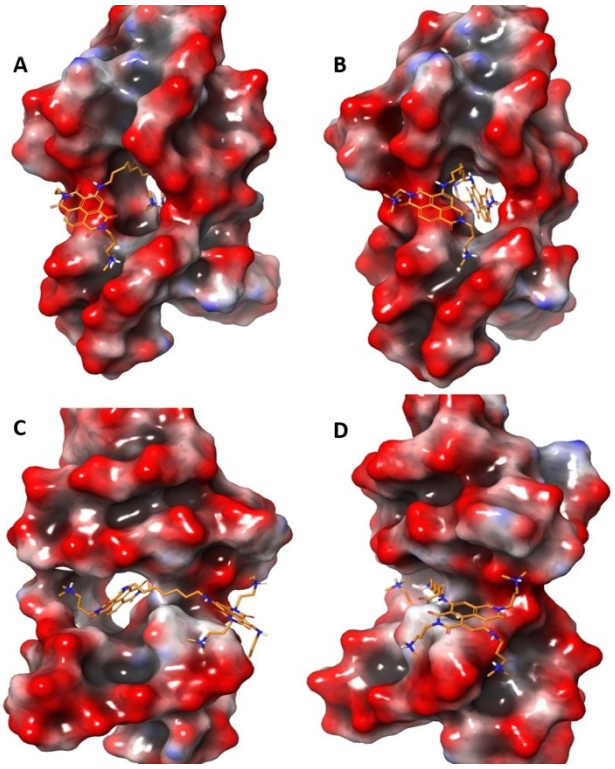

Figure 6. Best poses from docking analysis. Two different views are shown. The ligands are shown in sticks. The carbon atoms of the ligand are depicted in orange: A) and B) dyad 2; C) and D) dyad 1, both on hTel46.

engaged in electrostatic interactions with the backbone phosphate groups, and the remaining forming H-bonding interactions with the carbonyl group of flanking adenines. In the dyads **1** and **2**, the nature of these interactions is largely maintained by the NDI in the pocket. Interestingly, the second unit on the dyads facilitates additional interactions with the DNA regions flanking the pocket: the ammonium groups engage the phosphate groups of the backbone mainly in electrostatic interactions, while stacking of the ammonium moiety with nucleotide basis provides additional stabilization. Importantly, the additional ammonium motif in the asymmetric **1**, favors additional binding interactions of the same type as described above, further strengthening binding.

The docking energy parameters recapitulate this situation, pointing to **1** as the best binder, followed by **2** and finally **4** and **3** (Glide Score shown in Table S5). Considering force field limitation and the simplicity of the model these results should be considered as a valid means to provide qualitative insights in the G4/ligand molecular recognition motifs. In our model, the second aromatic unit plays an active role in binding by targeting the region of G4 that is proximal to the binding pocket. In this framework, substituent groups on this unit modulate affinities by forming additional stabilizing interactions.

Discussion

To gain deeper insight in the different behavior of NDI monomers and dyads at the biological level, with only the dyads able to induce a DNA damage response at the telomeric level, we investigated their interaction with a dimeric telomere G4 as it can afford additional crucial information. The selected sequence hTel45 indeed represents a more complete model of telomeric DNA as it features the binding site at the interface of the two G4s lacking in hTel22. hTel45 adopts in K^+-rich solution a dimeric hybrid-1/hybrid-2 G4 structure[8b], in which we can envisage the presence of a higher number of binding sites with respect to the hTel22 monomeric G4 model including the binding site at the interface of the two G4s. The space between the two G4 units consists in a pocket confined by a bridging T22T23 A24 sequence and two lateral loops, one of the hybrid-1 G4 (T10T11 A12) and one of the hybrid-2 G4 (T34T35 A36). The short sequence hTel22 adopts a hybrid-1 conformation as main conformer in K^+-rich solution[6] and presents an adenine residue at the 5′ end that can reduce accessibility to one external G tetrad as well as participate in ligand binding. As expected, all experimental data of the 4 NDIs examined confirm higher stoichiometries for hTel45 complexes compared to hTel22. Generally, fitting of the spectroscopic data converges with more than one model. Statistical parameters afforded by Reactlab Equilibria, comparison with global analysis data of the fluorescence decays and comparison with the ITC data allowed to assign a model affording an overall coherent complexation scheme. We do not see any "doubling" effect in the number of ligands going from hTel22 to hTel45 neither a situation with "doubling plus one" due to the hypothetical new binding site at the interface between the two hybrid G4s.

Noticeably, only in the case of binding of the dyads **1** and **2** to the dimeric hTel45, the situation evolves with low excess of DNA to a single complex with 1:1 stoichiometry, which is indicative of a unique site displaying the highest affinity. In all other cases, **1**–**4** with hTel22 and monomeric ligands **3**–**4** with hTel45, complexes of higher stoichiometry were found even in the presence of excess DNA. To identify this unique site, we make a close up on other information available especially for the dyads.

For the homologous dyad **2**, we observe significant differences comparing the data for the two DNAs starting from the different stoichiometry for the complexes with the lowest ligand number. Binding to hTel45 is enthalpy driven while the binding to hTel22 is entropy driven. In the case of hTel45 unfavorable entropy may result from a strong reduction of the degrees of freedom of the dyad in the complex while the high enthalpy change likely reflects many interactions between the dyad and the host. Modeling indeed confirms that the dyad establishes several interactions in the binding pocket at the interface involving both NDI units thus reducing the degrees of freedom of the dyad. A new lifetime value of 0.75 ns appears with a fractional concentration that closely follows the trend of the 1:1 complex concentration for the global decay analysis. Single fluorescence decay fit with excess DNA indicates that the dyad in the binding site with 0.75 ns lifetime has a fractional concentration of 94%, so almost all dyad molecules reside in this site. According to the binding constants at the end of titration about 80% of the dyads resides in the 1:1 complex the others in the complex with 4:1 stoichiometry. We interpret the new lifetime of 0.75 ns in hTel45 complexes with the dyad being in the pocket between the G4's where we observe one NDI unit involved in stacking with A and the other not according to the modeling study. We know from literature that electron transfer to an excited fluorophore is less efficient for A than G thus giving a rationale for the longer 0.75 ns lifetime.[23b] Further compelling evidence of the new site at the G4 interface occupied by the dyad in the hTel45 complex comes from the appearance of an intense induced CD signal in the visible. Induced CD for non-chiral molecules such as the NDIs studied can derive from the restriction of conformational freedom due to intermolecular interactions in the complex with the chiral substrate, *ie* G4, and from the coupling of the transition dipole moments of the chromophores in the interacting system: this interaction must induce a specific and preferential mutual orientation between the interacting molecules, such that the induced CD signals are not canceled out by opposite contributions of other random orientations. The modeling study and the thermodynamic parameters indicate indeed that the binding pocket between two G4s offers an environment where both units of the dyad establish several interactions with the G4 skeleton in a crowded environment composed by the TTA bridging bases and the bases of the two lateral loops. In such a situation the dyad is blocked keeping the transition dipole moments of the two chromophores in a specific orientation giving origin to the strong induced ellipticity signal. In the case of the 2:1 complex of dyad **2** with hTel22 the energy penalty for the disruption of the mutual NDI interaction is not fully compensated by the establishment of new interactions with the DNA. The favorable entropy can be due either to the dyad being less rigid in the binding site as a low number of interactions is occurring or an increase in number of conformations of the complexes. The latter is suggested by CD changes in the UV indicative of the formation of antiparallel complexes together with the hybrid-1 complexes. In the 2:1 complex of hTel22 about 90% of the dyads occupy two sites with a short lifetime of 0.3 ns, a value representing the lower instrumental limit. This value indicates quenching is very efficient and suggests better interaction with the quenching purines, in particular G. Likely the dyads reside in the two regions formed by the lateral loops flanking the G-tetrads where we can envisage close proximity to G units. The induced CD signal in hTel22 is almost inexistent and confirms complexation does not block the two NDIs of the dyad in a specific position as they experience a lower number of interactions with the G4 and more conformational freedom.

As to the dyad **1** we observe the existence of a 1:1 complex for hTel45 with a significantly higher log*K* value of 7.11 and this species is not detected for hTel22 characterized by much lower log*K* value for the exclusive 2:1 complex. Binding to hTel22 is only entropy driven while binding to hTel45 is enthalpy and entropy driven. Noticeably, CD VIS acquires importance only in the hTel45 complex and in shape is similar to the induced CD

spectrum of the dyad **2** complexed to hTel45. These features suggest binding of the dyad in the pocket where the molecule experiences a rigid environment as suggested by the modeling. However, the two lifetimes of 1.2 and 5.15 ns for excess hTel45 with fractional concentrations of 0.61 and 0.39 indicate the existence of two sites with similar affinity in the 1:1 complex. Note that at the end of the titration about 80% of the molecules resides in the 1:1 complex and 20% in the 2:1 complex with hTel45. The new lifetime of 1.2 ns agrees with the binding features emerging from the modeling study. The tetrasubstituted unit in the binding pocket at the interface is at a center-to-center distance of 9–10 Å from either A or G bases, a distance compatible with electron transfer and depending further on the orientation of the donor and acceptor in this rigid environment. As to the second site with the long lifetime, 5.15 ns lifetime in common with hTel22, we hypothesize that binding of the tri-substituted unit by stacking with a G-tetrad allows the tetra-substituted unit to protrude toward the grooves thanks to the heptyl linker where major solvent protection can be expected or electron transfer is not allowed due to unfavorable orientation. A similar situation has been proposed for dyad **1** binding to hTel22 exhibiting a lifetime of 5.2 ns.[17b] Dyad **1** engages only in a 2:1 complex with hTel22 but we observe three lifetimes corresponding to three binding sites in the presence of excess DNA with about 90% of the molecules residing in the 2:1 complex. Complex heterogeneity is also supported by the very negative -TΔS value. CD VIS is almost inexistent in the hTel22 complex confirming dyad flexibility in the hTel22 complexes.

As to the monomeric ligands there is no evolution to a situation with a 1:1 complex, neither for hTel22 nor for hTel45, and the three lifetimes in the presence of excess DNA confirm heterogeneity in binding sites in the complexes with 2:1 stoichiometry. Likely binding occurs also at the binding pocket not being however a preferential site. Overall, to confirm and get deeper insight in binding at the interface of two telomeric G4s it was necessary to put together the information of experimental complementary techniques and modeling. From the study it emerges that the binding pocket indeed offers an additional binding site to the NDI ligands examined but only in the case of the dyads it becomes a preferential binding site indicating the importance of the ligand structure. The dyads ability to engage in a 1:1 complex occupying the pocket at the interface may offer a rationale for their superior performance to induce the cellular DNA damage response at the telomeric level compared to the monomeric NDIs.[17b]

Conclusions

We investigated NDI monomers and dyads as ligands of a dimeric hybrid-1/hybrid-2 G4 structure of human telomeric DNA comparing the results with those of the model monomeric hybrid-1 G4. Combination of time-resolved optical spectroscopic techniques with isothermal titration calorimetry and molecular modelling allowed to obtain new information on binding in the pocket at the interface of the two telomeric G4s. Time-resolved fluorescence data were read in the light of needful information on the complexation model and the free and complexed species distribution in solution. Ligand fluorescence lifetime data as well as induced circular dichroism afforded clues on the occupancy of the binding site at the interface. Thermodynamic parameters further confirmed the theory as they drastically change for the dyad complexes of the monomeric and dimeric telomeric G4 with enthalpy becoming the driving factor for binding. The ligand structure plays a crucial role as only the dyads engage in complexes of the dimeric G4 with 1:1 stoichiometry establishing multiple interactions with the DNA skeleton at the G4 interface. Further, affinity of the dyads engaging in 1:1 complexes at the junction between the two G4 domains is higher for hTel45 compared to the affinity per binding site in the hTel22 complexes. Our attempt to rationalize the biological data showing a superior behaviour of the dyads in inducing telomeric DNA damage response required the comparison of data for the two types of DNA. The approach presented resulted to be a winning strategy to obtain important information on binding in higher order structures where NMR and crystallographic data often fail to give the expected output and importantly can be extended to other multimeric G4s like those present in some oncogene promotors.

Acknowledgements

We gratefully acknowledge the Italian Association for Cancer Research for financial support. [Grant 14708 to M. F.]. We are grateful to Prof. Zhi-Shu Huang (Sun Yatsen University, Guangzhou 510006, China) for sharing the pdb file of tel46G4 published in Ref. [12].

Conflict of Interest

The authors declare no conflict of interest.

Keywords: Human Telomeric DNA · Multimeric G-quadruplexes · Naphthalene diimide dyads · Fluorescence Lifetime and Multiwavelength Global Analysis · Isothermal Titration Calorimetry

[1] M. L. Bochman, K. Paeschke, V. A. Zakian, *Nat. Rev. Genet.* **2012**, *13*, 770–780.
[2] a) G. Biffi, D. Tannahill, J. McCafferty, S. Balasubramanian, *Nat. Chem.* **2013**, *5*, 182–186; b) D. Rhodes, H. J. Lipps, *Nucl. Acids Res.* **2015**, *43*, 8627–8637; c) A. Henderson, Y. Wu, Y. C. Huang, E. A. Chavez, J. Platt, F. B. Johnson, R. M. Brosh, D. Sen, P. M. Lansdorp, *Nucl. Acids Res.* **2014**, *42*, 860–869; d) R. Hansel-Hertsch, M. Di Antonio, S. Balasubramanian, *Nat. Rev. Mol. Cell Biol.* **2017**, *18*, 279–284; e) L. I. Jansson, J. Hentschel, J. W. Parks, T. R. Chang, C. Lu, R. Baral, C. R. Bagshaw, M. D. Stone, *Proc. Nat. Acad. Sci.* **2019**, *116*, 9350.
[3] K. A. Lewis, D. S. Wuttke, *Structure* **2012**, *20*, 28–39.
[4] a) D. J. Patel, A. T. Phan, V. Kuryavyi, *Nucl. Acids Res.* **2007**, *35*, 7429–7455; b) P. Martinez, M. A. Blasco, *J. Cell Biol.* **2017**, *216*, 875–887.
[5] a) S. Neidle, *J. Med. Chem.* **2016**, *59*, 5987–6011; b) S. Asamitsu, T. Bando, H. Sugiyama, *Chem. Eur. J.* **2019**, *25*, 417–430.

[6] A. Ambrus, D. Chen, J. Dai, T. Bialis, R. A. Jones, D. Yang, *Nucl. Acids Res.* **2006**, *34*, 2723–2735.
[7] a) M. H. Hu, S. B. Chen, B. Wang, T. M. Ou, L. Q. Gu, J. H. Tan, Z. S. Huang, *Nucl. Acids Res.* **2017**, *45*, 1606–1618; b) J. F. Zhao, Q. Q. Zhai, *Bioorganic Chem.* **2020**, *103*, 104229; c) C. Gao, Z. Liu, H. T. Hou, J. Q. Ding, X. Chen, C. B. Xie, Z. B. Song, Z. Hu, M. Q. Feng, H. I. Mohamed, S. Z. Xu, G. N. Parkinson, S. Haider, D. G. Wei, *Nucl. Acids Res.* **2020**, *48*, 11259–11269; d) B. Maji, K. Kumar, K. Muniyappa, S. Bhattacharya, *Org. Biomol. Chem.* **2015**, *13*, 8335–8348.
[8] a) R. Takeuchi, T. Zou, D. Wakahara, Y. Nakano, S. Sato, S. Takenaka, *Chem. Eur. J.* **2019**, *25*, 8691–8695; b) L. Petraccone, J. O. Trent, J. B. Chaires, *J. Am. Chem. Soc.* **2008**, *130*, 16530–16532; c) H. T. Le, W. L. Dean, R. Buscaglia, J. B. Chaires, J. O. Trent, *J. Phys. Chem. B* **2014**, *118*, 5390–5405.
[9] Q. Zhang, Y. C. Liu, D. M. Kong, D. S. Guo, *Chem. Eur. J.* **2015**, *21*, 13253–13260.
[10] a) A. Cummaro, I. Fotticchia, M. Franceschin, C. Giancola, L. Petraccone, *Biochimie* **2011**, *93*, 1392–1400; b) M. Tera, T. Hirokawa, S. Okabe, K. Sugahara, H. Seimiya, K. Shimamoto, *Chem. Eur. J.* **2015**, *21*, 14519–14528; c) T. Z. Ma, M. J. Zhang, T. C. Liao, J. H. Li, M. Zou, Z. M. Wang, C. Q. Zhou, *Org. Biomol. Chem.* **2020**, *18*, 920–930; d) C. Q. Zhou, T. C. Liao, Z. Q. Li, J. Gonzalez-Garcia, M. Reynolds, M. Zou, R. Vilar, *Chem. Eur. J.* **2017**, *23*, 4713–4722.
[11] C. Zhao, L. Wu, J. Ren, Y. Xu, X. Qu, *J. Am. Chem. Soc.* **2013**, *135*, 18786–18789.
[12] a) V. Pirota, M. Nadai, F. Doria, S. N. Richter, *Molecules* **2019**, *24*; b) C. Röger, F. Würthner, *J. Org. Chem.* **2007**, *72*, 8070–8075; c) N. Sakai, J. Mareda, E. Vauthey, S. Matile, *Chem. Commun.* **2010**, *46*, 4225–4237; d) F. Doria, M. Nadai, M. Zuffo, R. Perrone, M. Freccero, S. N. Richter, *Chem. Commun.* **2017**, *53*, 2268–2271.
[13] a) E. Salvati, F. Doria, F. Manoli, C. D'Angelo, A. Biroccio, M. Freccero, I. Manet, *Org. Biomol. Chem.* **2016**, *14*, 7238–7249; b) F. Doria, I. Manet, V. Grande, S. Monti, M. Freccero, *J. Org. Chem.* **2013**, *78*, 8065–8073.
[14] a) G. W. Collie, R. Promontorio, S. M. Hampel, M. Micco, S. Neidle, G. N. Parkinson, *J. Am. Chem. Soc.* **2012**, *134*, 2723–2731; b) F. Cuenca, O. Greciano, M. Gunaratnam, S. Haider, D. Munnur, R. Nanjunda, W. D. Wilson, S. Neidle, *Bioorg. Med. Chem. Lett.* **2008**, *18*, 1668–1673; c) M. Micco, G. W. Collie, A. G. Dale, S. A. Ohnmacht, I. Pazitna, M. Gunaratnam, A. P. Reszka, S. Neidle, *J. Med. Chem.* **2013**, *56*, 2959–2974; d) M. Arevalo-Ruiz, F. Doria, E. Belmonte-Reche, A. De Rache, J. Campos-Salinas, R. Lucas, E. Falomir, M. Carda, J. M. Perez-Victoria, J. L. Mergny, M. Freccero, J. C. Morales, *Chem. Eur. J.* **2017**, *23*, 2157–2164.
[15] M. Gunaratnam, M. de la Fuente, S. M. Hampel, A. K. Todd, A. P. Reszka, A. Schatzlein, S. Neidle, *Bioorg. Med. Chem.* **2011**, *19*, 7151–7157.
[16] a) V. Pirota, C. Platella, D. Musumeci, A. Benassi, J. Amato, B. Pagano, G. Colombo, M. Freccero, F. Doria, D. Montesarchio, *Int. J. Biol. Macromol.* **2021**, *166*, 1320–1334; b) C. Platella, V. Pirota, D. Musumeci, F. Rizzi, S. Iachettini, P. Zizza, A. Biroccio, M. Freccero, D. Montesarchio, F. Doria, *Int. J. Mol. Sci.* **2020**, *21*, 1964.
[17] a) F. Doria, A. Oppi, F. Manoli, S. Botti, N. Kandoth, V. Grande, I. Manet, M. Freccero, *Chem. Commun.* **2015**, *51*, 9105–9108; b) F. Doria, E. Salvati, L. Pompili, V. Pirota, C. D'Angelo, F. Manoli, M. Nadai, S. N. Richter, A. Biroccio, I. Manet, M. Freccero, *Chem. Eur. J.* **2019**, *25*, 11085–11097.
[18] a) P. Changenet-Barret, T. Gustavsson, D. Markovitsi, I. Manet, *ChemPhysChem* **2016**, *17*, 1264–1272; b) A. Shivalingam, M. A. Izquierdo, A. L. Marois, A. Vysniauskas, K. Suhling, M. K. Kuimova, R. Vilar, *Nat. Commun.* **2015**, *6*, 8178.
[19] a) A. Arora, S. Maiti, *J. Phys. Chem. B* **2009**, *113*, 8784–8792; b) A. Arora, S. Maiti, *J. Phys. Chem. B* **2008**, *112*, 8151–8159.
[20] a) C. Liu, B. Zhou, Y. Geng, D. Yan Tam, R. Feng, H. Miao, N. Xu, X. Shi, Y. You, Y. Hong, B. Z. Tang, P. Kwan Lo, V. Kuryavyi, G. Zhu, *Chem. Sci.* **2019**, *10*, 218–226; b) R. D. Gray, J. Li, J. B. Chaires, *J. Phys. Chem. B* **2009**, *113*, 2676–2683.
[21] X. Xie, O. Reznichenko, L. Chaput, P. Martin, M.-P. Teulade-Fichou, A. Granzhan, *Chem. Eur. J.* **2018**, *24*, 12638–12651.
[22] H.-A. Wagenknecht, *Nat. Prod. Rep.* **2006**, *23*, 973–1006.
[23] a) A. K. Thazhathveetil, M. A. Harris, R. M. Young, M. R. Wasielewski, F. D. Lewis, *J. Am. Chem. Soc.* **2017**, *139*, 1730–1733; b) K. Kawai, Y. Osakada, M. Fujitsuka, T. Majima, *J. Phys. Chem. B* **2007**, *111*, 2322–2326.
[24] Sigmoidicty is represented by the c parameter, obtained multiplying the DNA concentration and the affinity constant.
[25] a) A. Funke, B Karg, J. Dickerhoff, D. Balke, S. Muller, K. Weisz, *ChemBioChem* **2018**, *19*, 505–512; b) X. Huang, L. Zhu, B. Wu, Y. Huo, N. Duan, D. Kong, *Nucl. Acids Res.* **2014**, *42*, 8719–8731.
[26] While these models are necessarily limited to a 1:1 ligand-receptor stoichiometry, mainly dictated by the requirement for docking calculations to return favourable binding energies, it may be hypothesized that high concentration conditions favour the occupation of other binding sites. In this case, the abundance of the ligands would be expected to overcome their limited affinity for this superficial site. As interacting chromophores we consider both NDI-NDI interaction and NDI-base interaction.

Manuscript received: April 26, 2021
Accepted manuscript online: June 21, 2021
Version of record online: July 7, 2021

